

LBT observations of compact star-forming galaxies with extremely high $[\text{O III}]/[\text{O II}]$ flux ratios: He I emission-line ratios as diagnostics of Lyman continuum leakage

Y. I. Izotov¹, T. X. Thuan² and N. G. Guseva¹

¹*Main Astronomical Observatory, Ukrainian National Academy of Sciences, Zabolotnoho 27, Kyiv 03143, Ukraine, izotov@mao.kiev.ua, guseva@mao.kiev.ua*

²*Astronomy Department, University of Virginia, P.O. Box 400325, Charlottesville, VA 22904-4325, txt@virginia.edu*

18 July 2017

ABSTRACT

We present Large Binocular Telescope spectrophotometric observations of five low-redshift ($z < 0.070$) compact star-forming galaxies (CSFGs) with extremely high emission-line ratios $\text{O}_{32} = [\text{O III}]\lambda 5007/[\text{O II}]\lambda 3727$, ranging from 23 to 43. Galaxies with such high O_{32} are thought to be promising candidates for leaking large amounts of Lyman continuum (LyC) radiation and, at high redshifts, for contributing to the reionization of the Universe. The equivalent widths $\text{EW}(\text{H}\beta)$ of the $\text{H}\beta$ emission line in the studied galaxies are very high, $\sim 350 - 520 \text{ \AA}$, indicating very young ages for the star formation bursts, < 3 Myr. All galaxies are characterized by low oxygen abundances $12+\log\text{O}/\text{H} = 7.46 - 7.79$ and low masses $M_{\star} \sim 10^6 - 10^7 M_{\odot}$, much lower than the M_{\star} for known low-redshift LyC leaking galaxies, but probably more typical of the hypothetical population of low-luminosity dwarf LyC leakers at high redshifts. A broad $\text{H}\alpha$ emission line is detected in the spectra of all CSFGs, possibly related to expansion motions of supernova remnants. Such rapid ionized gas motions would facilitate the escape of the resonant $\text{Ly}\alpha$ emission from the galaxy. We show that high O_{32} may not be a sufficient condition for LyC leakage and propose new diagnostics based on the He I $\lambda 3889/\lambda 6678$ and $\lambda 7065/\lambda 6678$ emission-line flux ratios. Using these diagnostics we find that three CSFGs in our sample are likely to have density-bounded H II regions and are thus leaking large amounts of LyC radiation. The amount of leaking LyC radiation is probably much lower in the other two CSFGs.

Key words: galaxies: dwarf – galaxies: starburst – galaxies: ISM – galaxies: abundances.

1 INTRODUCTION

Recent studies of low-redshift compact star-forming galaxies (CSFGs) found in the Sloan Digital Sky Survey (SDSS) demonstrated that they are low-mass and low-metallicity galaxies with star formation occurring in short bursts of a few million years duration (e.g. Cardamone et al. 2009; Izotov, Guseva & Thuan 2011; Izotov et al. 2016c). In the literature, and depending on their redshifts, subsets of these galaxies have been variously called blue compact dwarf (BCD) galaxies at redshifts $z < 0.1$ (Loose & Thuan 1986; Thuan 2008) because of their blue colours, “Green peas” (GPs) which at redshifts of $\sim 0.1 - 0.3$ appear green on composite SDSS images (Cardamone et al. 2009) and luminous compact galaxies (LCGs) with diverse colours in the wider redshift range from 0 to ~ 0.6 (Izotov et al. 2011).

These properties together with the fact that CSFGs

and high-redshift star-forming galaxies (SFGs) follow similar mass-metallicity and luminosity-metallicity relations suggest that CSFGs are good local counterparts of the Lyman-alpha emitting (LAE) galaxies and Lyman-break galaxies (LBGs) (Izotov et al. 2015). The presence of strong emission lines in the optical spectra of the H II regions of CSFGs, powered by $\sim 10^3 - 10^5$ O-stars which produce plenty of ionizing radiation, make them promising candidates for leaking ionizing radiation into the intergalactic medium (IGM) (Cardamone et al. 2009; Izotov et al. 2011; Jaskot & Oey 2013; Stasińska et al. 2015). It is indeed thought that dwarf galaxies with similar properties are responsible for the reionization of the Universe at redshifts $z = 5 - 10$ (Ouchi et al. 2009; Wise & Chen 2009; Mitra et al. 2013; Yajima et al. 2011; Bouwens et al. 2015a).

Many CSFGs are characterised by high line ratios O_{32}

= $[\text{O III}]\lambda 5007/[\text{O II}]\lambda 3727$, reaching values of up to 60 in some galaxies (Stasińska et al. 2015). Such high values may indicate that their H II regions are density-bounded, allowing escape of ionizing radiation into the IGM, as suggested e.g. by Jaskot & Oey (2013), Nakajima & Ouchi (2014) and Nakajima et al. (2016). However, that is not the only explanation. A high O_{32} can also be caused by a low metallicity, a high ionization parameter or a hard ionizing radiation (Jaskot & Oey 2013; Stasińska et al. 2015). From various emission-line diagnostics, Stasińska et al. (2015) reached the conclusion that CSFGs are in general opaque to ionizing radiation, and that they have low absolute escape fractions, not exceeding 10 percent.

Direct observations of CSFGs at UV wavelengths below the Lyman limit were needed to check for the amount of escaping Lyman continuum (LyC) radiation. Izotov et al. (2016a,b) detected escaping LyC radiation with escape fraction $f_{\text{esc}} = 7 - 13$ percent in five CSFGs at redshifts $z \sim 0.3$, using the Cosmic Origin Spectrograph (COS) aboard the *Hubble Space Telescope* (*HST*). Objects need to be in the redshift range of $\sim 0.3 - 0.4$ so as to shift the LyC spectral region into the wavelength range where the COS is most sensitive. These LyC leaking galaxies together with four other known LyC leakers at lower redshifts (Leitet et al. 2013; Borthakur et al. 2014; Leitherer et al. 2016) are all characterised by a relatively low $\text{O}_{32} \lesssim 8$.

Our team has been awarded *HST* time in Cycle 24 to observe CSFGs at $z \sim 0.3 - 0.4$, with more extreme O_{32} , $\sim 10 - 30$ (Program GO14635, PI: Y.I.Izotov), but the data are not yet obtained. The number of such extreme galaxies at $z \gtrsim 0.3$, suitable for *HST* observations, is very limited in the SDSS because the majority of them are very faint. Many more brighter extreme SDSS CSFGs can be found at lower redshifts, with $z \leq 0.3$. However, their low redshifts prevent them from being observed with the *HST* in the Lyman limit range, because this range is not shifted into the spectral region where the COS is most sensitive. Therefore, indirect methods for selecting candidate CSFGs with potential LyC leakage are needed. In the UV range, the profile shape of the $\text{Ly}\alpha$ emission line has been proposed as a diagnostic for LyC leaking (Verhamme et al. 2017). However, UV observations of low-redshift objects can only be done from space and are not readily available. The aim of this paper is to identify line ratio diagnostics in the optical range which, in addition to the high O_{32} ratio, can be used to select potential LyC leakers from the SDSS. The best candidates can then be followed-up in the UV with the *HST* to study their $\text{Ly}\alpha$ emission line profile and low-ionization (LIS) absorption lines, put constraints on the optical depth of the LyC and derive the escape fraction of leaking ionizing radiation.

In this paper, we have used Large Binocular Telescope (LBT)¹ spectroscopic observations with high signal-to-noise

ratio of five CSFGs selected from the SDSS to have extremely high $\text{O}_{32} = 23 - 43$, to develop such optical diagnostics. In Section 2 we describe the sample of CSFGs and the criteria used for their selection. The observations and data reduction are described in Section 3. Element abundances are derived in Section 4. In Section 5 we study the $\text{H}\alpha$ broad-line emission. The emission-line diagnostics, which can be used to identify potential LyC leakers, are discussed in Section 6. We summarize our main results in Section 7.

2 SELECTION OF CSFGS AND THEIR GLOBAL CHARACTERISTICS

From the spectroscopic data base of the SDSS Data Release 12 (DR12) (Alam et al. 2015), Izotov et al. (2016c) have constructed a sample of ~ 15000 CSFGs. These objects were selected by their compactness, strong emission lines and absence of AGN spectral features. The sample includes 26 galaxies with extremely high O_{32} , > 20 . Out of these, five galaxies have been chosen for LBT observations. Their coordinates, O_{32} , redshifts and apparent SDSS g magnitudes are presented in Table 1. The composite SDSS images of the selected galaxies are shown in Fig. 1. They are all characterised by a compact nearly unresolved structure. All five galaxies were detected by *Galaxy Evolution Explorer* (*GALEX*) in the UV range and by *Wide-field Infrared Survey Explorer* (*WISE*) in the mid-infrared (MIR) range. Their UV and MIR apparent magnitudes are shown in Table 1. Out of the five CSFGs, three objects, J0159+0751, J1032+4919 and J1205+4551, have very red *WISE* colours, $W1 - W2 > 1.5$ mag, indicating the presence of hot dust (Izotov et al. 2014a). The $W1 - W2$ colours of the remaining two CSFGs, J1355+4651 and J1608+3528, are however not so red (< 1 mag), implying less dust heating.

The location of the five selected galaxies in the $[\text{O III}]\lambda 5007/\text{H}\beta - [\text{N II}]\lambda 6584/\text{H}\alpha$ diagnostic diagram (Baldwin, Phillips & Terlevich 1981) is shown in Fig. 2a by filled stars. It is seen that four out of the five CSFGs are more extreme objects compared to the five strong LyC leakers from Izotov et al. (2016a,b) (large open circles), to the confirmed $\text{Ly}\alpha$ emitting GPs of Yang et al. (2017) (small open circles) and to the entire sample of CSFGs (dark-grey dots, Izotov et al. 2016c). Only one galaxy, J1205+4551, with a higher $[\text{N II}]\lambda 6584/\text{H}\alpha$ ratio and a lower $[\text{O III}]\lambda 5007/\text{H}\beta$ ratio, has properties similar to the most extreme LyC leakers and $\text{Ly}\alpha$ emitting GPs. The solid line derived by Kauffmann et al. (2003) separates SFGs from active galactic nuclei (AGN). All five CSFGs are located in the SFG region, implying that their interstellar medium is ionized by hot stars in the star-forming regions. However, they lie somewhat below the main sequence defined by the other SFGs in Fig. 2a, a consequence of their lower metallicities.

In Fig. 2b we compare the locations in the $\text{O}_{32} - \text{R}_{23}$ ($\text{R}_{23} = \{[\text{O II}]\lambda 3727 + [\text{O III}]\lambda 4959 + [\text{O III}]\lambda 5007\}/\text{H}\beta$) diagram of CSFGs possessing extremely high O_{32} (filled stars) with those of high-redshift LAEs that are potential LyC leakers (Nakajima & Ouchi 2014; Nakajima et al. 2016) (open triangles), of known $z \sim 0.3$ LyC leakers (large open circles, Izotov et al. 2016a,b), of LyC leaking galaxies at $z < 0.1$ (open squares, Leitert et al. 2013; Borthakur et al. 2014; Leitherer et al. 2016), and of $\text{Ly}\alpha$ emitting GPs (small

¹ The LBT is an international collaboration among institutions in the United States, Italy and Germany. LBT Corporation partners are: The University of Arizona on behalf of the Arizona university system; Istituto Nazionale di Astrofisica, Italy; LBT Beteiligungsgesellschaft, Germany, representing the Max-Planck Society, the Astrophysical Institute Potsdam, and Heidelberg University; The Ohio State University, and The Research Corporation, on behalf of The University of Notre Dame, University of Minnesota and University of Virginia.

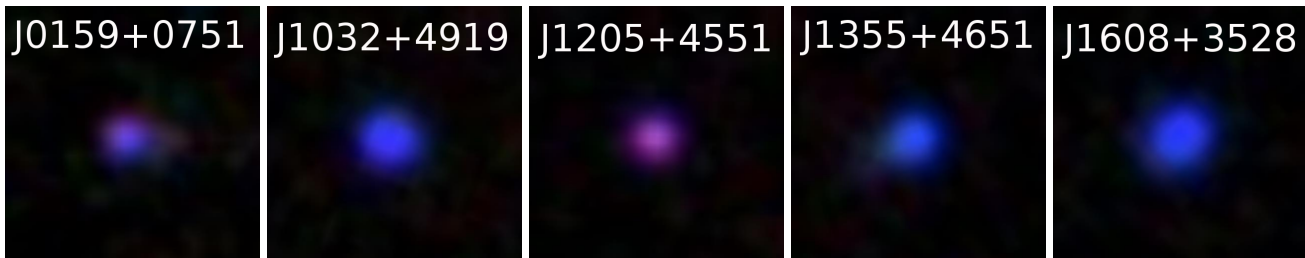


Figure 1. The $12'' \times 12''$ SDSS images of CSFGs with extremely high O_{32} .

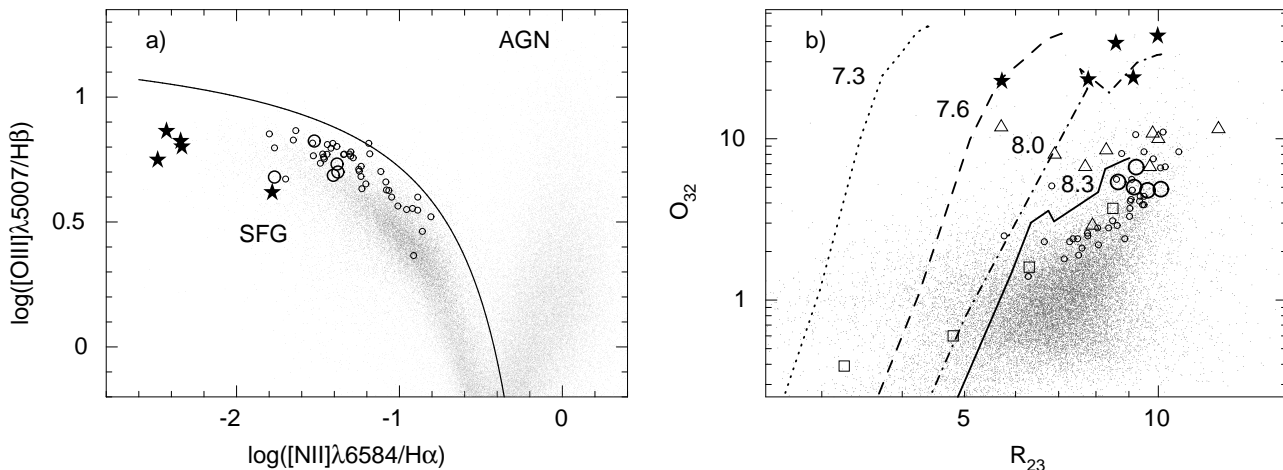


Figure 2. a) The BPT diagnostic diagram (Baldwin, Phillips & Terlevich 1981) for narrow emission-line galaxies. CSFGs with extremely high O_{32} (this paper) are shown by filled stars. For comparison, LyC leaking galaxies (Izotov et al. 2016a,b) and confirmed Ly α leakers (Yang et al. 2017) are represented by open large and small circles, respectively. Also shown are CSFGs from the SDSS DR12 (dark-grey dots, Izotov et al. 2016c) and SDSS DR7 narrow emission-line galaxies (light-grey dots). The solid line by Kauffmann et al. (2003) separates SFGs from active galactic nuclei (AGNs). b) The O_{32} - R_{23} diagram for SFGs, where $R_{23} = ([O II] 3727 + [O III] 4959 + [O III] 5007)/H\beta$. CSFGs with extreme O_{32} (this paper) are shown by filled stars. The location of $z \sim 0.3$ LyC leaking galaxies (Izotov et al. 2016a,b) and known low-redshift ($z < 0.1$) LyC leaking galaxies (Leitner et al. 2013; Borthakur et al. 2014; Leitherer et al. 2016) are shown by large open circles and open squares, respectively. For comparison, high- z Ly α emitting galaxies (LAEs) by Nakajima & Ouchi (2014) and Nakajima et al. (2016) (open triangles), confirmed low- z Ly α emitting galaxies (Yang et al. 2017) (small open circles) are shown. SDSS CSFGs (Izotov et al. 2016c) are shown by grey dots. Theoretical predictions of optically-thick (case B) photoionized H II region models with log of filling factor of -0.5 and with the production rate of ionizing radiation $Q = 10^{53} \text{ s}^{-1}$ for four values of the oxygen abundance $12+\log O/H = 7.3, 7.6, 8.0,$ and 8.3 are shown by dotted, dashed, dash-dotted and solid lines, respectively.

open circles, Yang et al. 2017). We show by dotted, dashed, dash-dotted and solid lines the evolutionary sequences predicted by CLOUDY photoionization models calculated for four values of the oxygen abundance (the $12+\log O/H$ value labels each curve), for H II regions ionized only by stellar radiation and that are optically thick (case B). Along the curves, higher modelled O_{32} values correspond to younger starburst ages and thus to more intense and harder ionizing radiation. It is seen that the selected galaxies are located far above the LAEs, at the extreme of the distribution for SDSS galaxies, implying that they may be good LyC leaking candidates. In Fig. 2b, they lie somewhat apart from the main sequence defined by the other CSFGs because of their lower metallicities. No galaxy with such extreme O_{32} has been studied until now.

The global characteristics of the CSFGs with extreme O_{32} , derived from their SDSS spectra and GALEX photometry, are shown in Table 2. The observed fluxes have been transformed to luminosities and absolute magnitudes, adopting luminosity distances (NED, Wright 2006) derived

with the cosmological parameters $H_0=67.1 \text{ km s}^{-1}\text{Mpc}^{-1}$, $\Omega_\Lambda=0.682$, $\Omega_m=0.318$ (Planck Collaboration XVI 2014). The $H\beta$ luminosities $L(H\beta)$ were derived from the extinction-corrected $H\beta$ fluxes measured in the SDSS spectra. Additionally, $L(H\beta)$ were also corrected for aperture effects using the relation $2.512^{r(\text{ap})-r}$, where r and $r(\text{ap})$ are respectively the SDSS r -band total magnitude and the magnitude within the round spectroscopic SDSS 3 arcsec aperture for galaxies in the SDSS-II and 2 arcsec aperture for galaxies in the SDSS-III. We have also derived extinction-corrected absolute AB SDSS g -band and GALEX FUV magnitudes.

Using a Monte Carlo method, we have calculated galaxy stellar masses by fitting the spectral energy distribution (SED) of the SDSS spectra corrected for extinction as derived from the observed hydrogen Balmer decrement from the same spectra. The spectral fluxes were also corrected for the finite size of the spectroscopic aperture by comparing the total SDSS r magnitude to the magnitude r_{ap} inside the aperture. The Monte Carlo method is described

Table 1. Observed characteristics of galaxies

Name	R.A.(J2000)	Dec.(J2000)	O ₃₂ ^a	<i>z</i>	<i>g</i> (mag)	<i>FUV</i> (mag)	<i>NUV</i> (mag)	W1 (mag)	W2 (mag)	W3 (mag)	W4 (mag)
J0159+0751	01:59:52.75	+07:51:48.90	39	0.0611	19.47	20.64	20.43	17.39	15.88	11.54	8.52
J1032+4919	10:32:56.72	+49:19:47.24	24	0.0442	18.67	20.26	20.25	16.60	15.08	10.50	7.42
J1205+4551	12:05:03.55	+45:51:50.94	23	0.0654	19.79	21.04	20.58	15.14	13.55	9.91	7.80
J1355+4651	13:55:25.64	+46:51:51.34	23	0.0281	19.22	20.54	20.66	17.86	17.39
J1608+3528	16:08:10.36	+35:28:09.30	43	0.0327	18.59	20.01	20.42	18.02	17.06	11.56	8.77

^aderived from the LBT spectra.

Table 2. Global characteristics of galaxies

Name	log M_*/M_\odot	log $L(\text{H}\beta)$ (log erg s ⁻¹)	SFR (M _⊙ yr ⁻¹)	M_g (mag)	M_{FUV} (mag)	12+logO/H
J0159+0751	6.69	40.93	1.9	-18.73	-17.56	7.54
J1032+4919	6.65	40.74	1.2	-18.01	-16.42	7.65
J1205+4551	6.84	41.11	2.9	-18.56	-17.31	7.46
J1355+4651	6.05	39.99	0.2	-16.68	-15.36	7.57
J1608+3528	7.04	40.41	0.6	-18.43	-17.01	7.79

e.g. in Izotov et al. (2011, 2014a). Briefly, a grid of instantaneous burst SEDs in a wide range of ages, ranging from 0 Myr to 15 Gyr, was calculated with the *Starburst99* code (Leitherer et al. 1999, 2014) to derive the SED of the galaxy stellar component. We adopted Padova stellar evolution tracks (Girardi et al. 2000), stellar atmosphere models by Lejeune, Buser & Cuisiner (1997), and the stellar initial mass function by Salpeter (1955). Then the stellar SED with any star-formation history can be obtained by integrating the instantaneous burst SEDs over time with a specified time-varying star formation rate. Given the electron temperature T_e in the H II region, we interpolated emissivities from Aller (1984) for the nebular continuum in the T_e range of 5000 – 20000K, including hydrogen and helium free-bound, free-free, and two-photon emission. The emission lines were added to the total, stellar and nebular, continuum with fluxes measured in the SDSS spectra. The star-formation history is approximated assuming a short burst with age < 10 Myr and a prior continuous star formation with a constant SFR.

It is seen from Table 2 that the selected galaxies are dwarf systems with low stellar masses M_* , ranging from $\sim 10^6$ to $\sim 10^7 M_\odot$. These stellar masses are ~ 2 orders of magnitude lower than the stellar masses of the $z \sim 0.3$ LyC emitters studied by Izotov et al. (2016a,b). Furthermore, their absolute magnitudes are ~ 2 mag fainter. The extreme CSFGs are much more metal-poor, with oxygen abundances 12+logO/H between 7.46 and 7.79 (see also section 4). Finally, the equivalent widths of the H β emission line in our five CSFGs are very high, $\sim 350 - 520\text{\AA}$ (see section 3) implying a very high efficiency of the ionizing photon production ξ . These properties are similar to those of some local BCDs (Thuan 2008) and of the hypothetical dwarf galaxies thought to be the main contributors to the reionization of the Universe at redshifts $z > 5$.

3 OBSERVATIONS AND DATA REDUCTION

In the course of four LBT runs in the period 2013 – 2016, we have obtained long-slit spectrophotometric observations in the wavelength range 3200 – 10000Å of the galaxies listed in Table 1 with the dual spectrograph MODS1², equipped with two 8022 pix \times 3088 pix CCDs. The G400L grating in the blue beam, with a dispersion of 0.5Å/pix, and the G670L grating in the red beam, with a dispersion of 0.8Å/pix, were used. Spectra were obtained with a 1.2 arcsec wide slit, resulting in a resolving power $R \sim 2000$.

Three or four 800 s subexposures were obtained for each galaxy, resulting in total exposures of 2400 s or 3200 s (Table 3). The airmass was small during the observations of three CSFGs (Table 3). However, it is somewhat larger (~ 1.4) during the observations of J1355+4651 and J1608+3528, so that their spectra may be affected by atmospheric refraction. Several spectrophotometric standard stars, obtained during the same nights with a 5 arcsec wide slit, were used for flux calibration and correction for telluric absorption lines in the red part of the spectra. Additionally, calibration frames of biases, flats and argon comparison lamps were obtained during the same nights.

Basic data reduction was done with the MODS Basic CCD Reduction package MODSCCDRED³, including bias subtraction and flat field correction. Subsequent data reduction including wavelength and flux calibration, and night sky background subtraction was done with IRAF⁴. Cosmic ray hits were manually removed from the background-

² This paper used data obtained with the MODS spectrographs built with funding from NSF grant AST-9987045 and the NSF Telescope System Instrumentation Program (TSIP), with additional funds from the Ohio Board of Regents and the Ohio State University Office of Research.

³ <http://www.astronomy.ohio-state.edu/MODS/Software/modsCCDRed/>

⁴ IRAF is distributed by the National Optical Astronomy Observatories, which are operated by the Association of Universities for

Table 3. Large Binocular Telescope observations

Name	Date	Instrument	Exposure (s)	Slit (arcsec)	Airmass
J0159+0751	2016-01-02	MODS1	3200	60×1.2	1.10
J1032+4919	2016-02-12	MODS1	2400	60×1.2	1.04
J1205+4551	2016-04-10	MODS1	3200	60×1.2	1.24
J1355+4651	2013-06-08	MODS1	2400	60×1.2	1.44
J1608+3528	2013-06-08	MODS1	2400	60×1.2	1.42

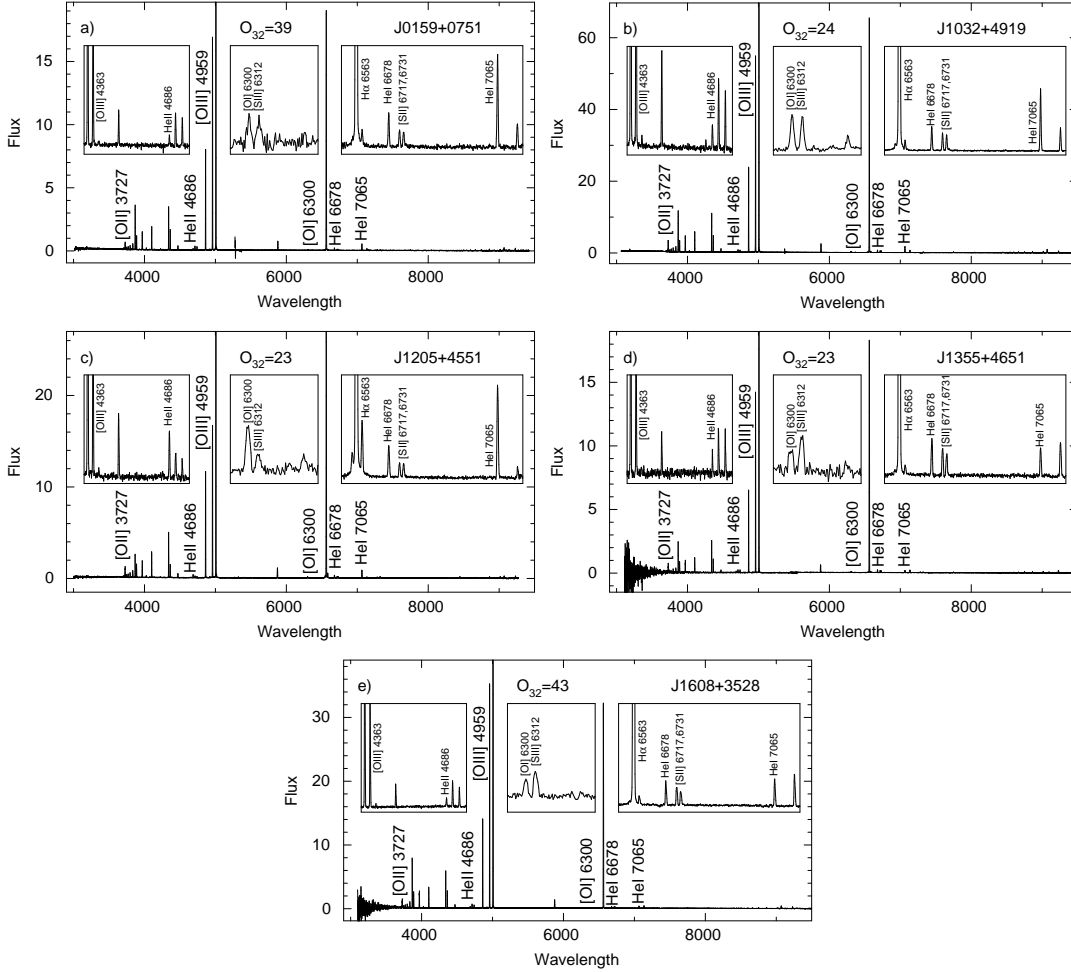


Figure 3. The rest-frame LBT spectra of CSFGs with extremely high O_{32} . Spectra were not corrected for extinction. Insets show expanded parts of spectral regions of interest in this paper. From left to the right, they cover the rest wavelength ranges $4325\text{\AA} - 4770\text{\AA}$, $6280\text{\AA} - 6380\text{\AA}$, and $6510\text{\AA} - 7155\text{\AA}$, respectively. Some interesting emission lines are labelled. Wavelengths are in \AA and fluxes are in $10^{-16} \text{ erg s}^{-1} \text{ cm}^{-2} \text{ \AA}^{-1}$.

subtracted frames which were then flux-calibrated. Individual subexposures for each object were co-added. Finally, one-dimensional spectra were extracted using the IRAF APALL routine.

The resulting rest-frame spectra are shown in Fig. 3. They are dominated by strong emission lines, suggesting active star formation. The strong $[\text{O III}] \lambda 4363$ emission line is

present in all spectra, allowing reliable abundance determination. Each panel includes three insets showing expanded parts of the spectra for a better view of particular emission lines of interest. There are several features of note. First, a weak broad component of the $\text{H}\alpha$ emission line is seen in the spectra of all CSFGs. Second, the strength of the $\text{He I } \lambda 7065$ emission line relative to the $\text{He I } \lambda 6678$ emission line varies in a large range. The former line depends more on collisional and fluorescent enhancement than the latter, and variations in their intensity ratios indicate that the physical conditions in the H II regions of the studied galaxies, as

Table 4. Extinction-corrected emission-line fluxes

Line	$100 \times I(\lambda)/I(H\beta)$				
	J0159+0751	J1032+4919	J1205+4551	J1355+4651	J1608+3528
3426.85 [Ne v]	0.72±0.11
3727.00 [O II]	16.15±0.55	27.86±0.89	18.26±0.59	24.08±0.59	16.85±0.62
3750.15 H12	4.43±0.26	3.62±0.17	4.42±0.19	3.82±1.20	4.12±0.37
3770.63 H11	5.10±0.26	4.70±0.19	4.78±0.20	4.98±1.95	4.96±0.36
3797.90 H10	6.83±0.29	6.01±0.22	6.19±0.23	8.23±1.52	6.49±0.40
3819.64 He I	1.29±0.12	0.99±0.06	1.19±0.07	...	1.51±0.21
3835.39 H9	8.64±0.33	7.86±0.27	8.15±0.28	8.57±1.31	7.79±0.40
3868.76 [Ne III]	56.68±1.78	53.67±1.67	24.25±0.76	49.73±1.69	60.19±1.90
3889.00 He I+H8	18.61±0.63	16.41±0.52	15.13±0.49	20.97±1.04	19.52±0.67
3968.00 [Ne III]+H7	35.47±1.11	33.85±1.04	24.56±0.77	33.75±1.38	33.06±1.06
4026.19 He I	2.13±0.11	1.97±0.08	1.97±0.08	2.56±0.26	1.71±0.10
4068.60 [S II]	...	0.79±0.06	0.65±0.06	...	0.61±0.02
4076.35 [S II]	...	0.18±0.05	0.30±0.06
4101.74 H δ	27.71±0.86	26.81±0.81	27.50±0.84	25.75±1.14	23.65±0.76
4120.84 He I	...	0.27±0.04	0.44±0.05	...	0.66±0.09
4143.76 He I	0.72±0.07	0.61±0.06	0.57±0.05	...	0.31±0.06
4227.20 [Fe V]	1.35±0.08	0.78±0.05	0.73±0.05	1.42±0.27	0.40±0.06
4340.47 H γ	48.29±1.43	47.56±1.39	46.99±1.38	44.63±1.46	43.36±1.28
4363.21 [O III]	22.90±0.68	20.85±0.61	12.87±0.38	18.13±0.57	18.96±0.56
4387.93 He I	0.89±0.09	0.49±0.04	0.49±0.05	1.08±0.16	0.60±0.05
4471.48 He I	4.12±0.15	4.10±0.13	4.02±0.13	3.56±0.16	3.59±0.12
4658.10 [Fe III]	...	0.38±0.05	0.58±0.05	...	0.28±0.03
4685.94 He II	1.58±0.09	1.16±0.06	3.24±0.11	1.61±0.10	1.89±0.08
4712.00 [Ar IV]+He I	4.54±0.15	3.15±0.10	2.15±0.05	3.67±0.16	4.95±0.16
4740.20 [Ar IV]	3.62±0.14	2.37±0.08	1.20±0.06	3.16±0.14	3.45±0.12
4861.33 H β	100.00±2.87	100.00±2.85	100.00±2.86	100.00±2.92	100.00±2.87
4921.93 He I	1.06±0.08	1.09±0.05	1.03±0.05	0.92±0.09	1.33±0.06
4958.92 [O III]	211.54±6.06	221.47±6.31	139.15±3.98	194.24±5.58	252.84±7.21
4988.00 [Fe III]	...	0.57±0.05
5006.80 [O III]	631.72±18.1	665.43±19.0	414.63±11.9	559.95±16.1	730.81±20.9
5015.68 He I	1.96±0.10	1.78±0.07	1.98±0.07	1.48±0.07	1.91±0.06
5411.52 He II	0.32±0.03
5517.71 [Cl III]	...	0.17±0.03
5537.88 [Cl III]	...	0.13±0.03
5754.64 [N II]	0.32±0.03
5875.60 He I	11.22±0.34	11.07±0.33	11.77±0.35	10.47±0.32	11.79±0.35
6300.30 [O I]	0.61±0.04	0.89±0.04	1.21±0.04	0.60±0.04	0.60±0.03
6312.10 [S III]	0.63±0.04	0.78±0.04	0.50±0.03	0.94±0.05	0.87±0.04
6363.80 [O I]	0.18±0.03	0.30±0.03	0.36±0.03	0.29±0.05	0.13±0.02
6548.10 [N II]	1.65±0.06	0.47±0.04	...
6562.80 H α	276.51±8.57	277.59±8.56	278.70±8.62	283.14±8.80	280.70±8.67
6583.40 [N II]	1.28±0.06	1.26±0.05	4.61±0.15	0.93±0.05	1.04±0.04
6678.10 He I	2.73±0.10	2.84±0.09	2.91±0.10	3.01±0.11	2.49±0.08
6716.40 [S II]	1.42±0.06	2.21±0.08	1.34±0.05	2.28±0.08	2.07±0.07
6730.80 [S II]	1.40±0.06	2.04±0.07	1.31±0.05	1.90±0.08	1.66±0.06
7065.30 He I	6.75±0.22	6.79±0.22	7.87±0.25	2.24±0.08	2.66±0.09
7135.80 [Ar III]	1.83±0.07	2.54±0.09	1.03±0.05	2.80±0.10	3.06±0.10
7281.21 He I	0.69±0.05	...	0.89±0.04	0.43±0.03	0.58±0.03
7319.90 [O II]	0.38±0.04	0.55±0.03	1.13±0.04	0.45±0.03	0.36±0.03
7330.20 [O II]	0.36±0.04	0.55±0.03	0.87±0.04	0.38±0.04	0.33±0.03
7751.12 [Ar III]	0.55±0.05	0.68±0.03	0.33±0.02	0.45±0.03	0.73±0.03
9069.00 [S III]	2.89±0.15	4.03±0.16	2.05±0.10	...	2.51±0.12
9530.60 [S III]	...	9.56±0.38	...	6.69±0.29	...
$C(H\beta)^a$	0.30±0.04	0.25±0.04	0.31±0.04	0.65±0.04	0.29±0.04
$F(H\beta)^b$	26.74±0.59	86.34±0.13	44.38±0.08	21.51±0.06	47.07±0.09
$EW(H\beta)^c$	347.00±1.00	438.50±0.63	519.40±0.90	494.00±1.40	406.60±0.78

^aExtinction coefficient. For $R(V) = 3.1$ it is linked to selective extinction by the relation $C(H\beta) = 1.47 \times E(B - V)$.^bObserved flux in 10^{-16} erg s^{-1} cm^{-2} .^cEquivalent width in \AA .

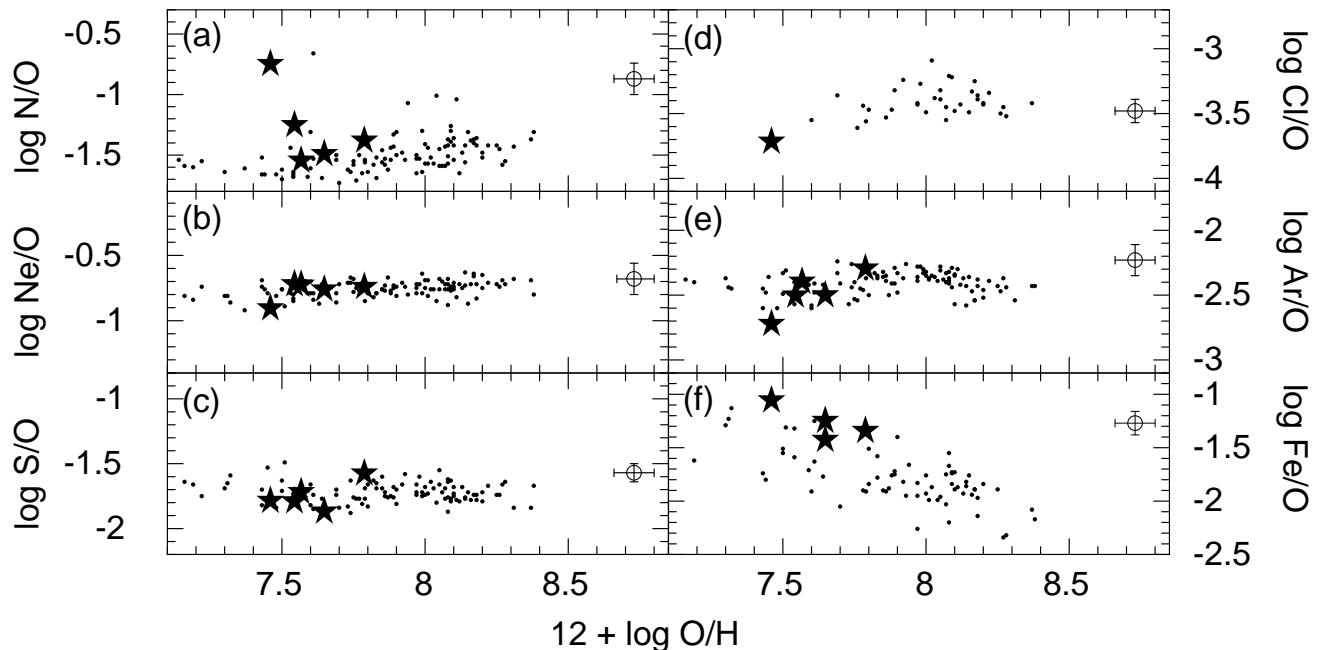


Figure 4. The dependences of heavy element abundance ratios (a) N/O, (b) Ne/O, (c) S/O, (d) Cl/O, (e) Ar/O and (f) Fe/O on the oxygen abundance $12+\log O/H$. CSFGs (this paper) are shown by filled stars. For comparison, BCDs from Izotov et al. (2006) and solar values by Lodders (2010) are shown by dots and open circles, respectively.

characterized by the electron number density and the optical depth, vary over a wide range. Third, an important feature of all spectra is the very weak [O II] $\lambda 3727$ emission line, as compared to the strong [O III] $\lambda 4959$, $\lambda 5007$ emission lines, resulting in unusually high O_{32} . Fourth, in one of the CSFGs, J1205+455, the high-ionization emission line [Ne V] $\lambda 3426\text{\AA}$ is detected, implying the presence of shocks produced by supernovae (Izotov et al. 2012).

Emission-line fluxes were measured using the IRAF SPLIT routine. The errors of the line fluxes were calculated from the photon statistics in the non-flux-calibrated spectra and adding a relative error of 1 percent in the absolute flux distribution of the spectrophotometric standards. The line flux errors were propagated in the calculations of the elemental abundance errors.

The observed fluxes were corrected for extinction with the extinction coefficient $C(H\beta)$, derived from the observed decrement of the hydrogen Balmer emission lines. We have adopted the Cardelli, Clayton & Mathis (1989) reddening law with $R(V) = A(V)/E(B-V) = 3.1$, where $A(V)$ and $E(B-V)$ are respectively the total extinction in the V band and the selective extinction. Recently, Izotov et al. (2017) by analyzing UV data of CSFGs, have shown that $R(V)$ may be lower than 3.1 in the UV range. However, in the optical range, at variance with the UV range, reddening laws with different $R(V)$'s are quite similar. For $R(V) = 3.1$, the total extinction is linked to $C(H\beta)$ by the relation $A(V) = 2.11 \times C(H\beta)$. The relations for other $R(V)$'s are given in Izotov et al. (2016a). We have also assumed that extinctions for nebular and stellar emission are equal, in accord with Izotov et al. (2017). The extinction-corrected emission line fluxes $I(\lambda)$ relative to the $H\beta$ fluxes multiplied by 100, the extinction coefficients $C(H\beta)$, the rest-frame equivalent

widths $EW(H\beta)$ and the observed $H\beta$ fluxes $F(H\beta)$ are listed in Table 4. We note that the $EW(H\beta)$ s of the studied CSFGs are very high, $\sim 350 - 520\text{\AA}$. They are among the highest ever measured in spectra of SFGs, indicating the bursting nature of the star formation and very young burst ages (< 3 Myr). For comparison, rest-frame $EW(H\beta)$ of $\sim 200\text{\AA}$ were found by Izotov et al. (2016a,b) for the five $z \sim 0.3$ LyC leakers, indicating somewhat larger burst ages.

We note, however, that the LBT spectra of J1355+4651 J1608+3528 obtained at high air masses are affected by atmospheric refraction. Indeed, the extinction coefficients $C(H\beta)$ for these two objects derived from the SDSS spectra with a wider 3 arcsec aperture are somewhat lower, being respectively 0.065 and 0.20. The respective values of O_{32} from the SDSS spectra are also lower, being 21 and 35. The effect of the atmospheric refraction is especially important in the LBT spectrum of J1355+4651, therefore its high $C(H\beta)$ of 0.65 is likely overestimated. Taking into account this refraction effect, we conclude that the overall dust extinction in the galaxies studied with the LBT is low.

4 ELEMENT ABUNDANCES

To determine element abundances, we follow the procedures of Izotov et al. (2006). We adopt a two-zone photoionized H II region model: a high-ionization zone with temperature $T_e(O III)$, where [O III], [Ne III], and [Ar IV] lines originate, and a low-ionization zone with temperature $T_e(O II)$, where [N II], [O II], [S II], and [Fe III] lines originate. As for the [S III] and [Ar III] lines, they originate in the intermediate zone between the high- and low-ionization regions. The temperature $T_e(O III)$ is calculated using the [O III] $\lambda 4363/(\lambda 4959$

Table 5. Ionic and total element abundances

Property	J0159+0751	J1032+4919	J1205+4551	J1355+4651	J1608+3528
$T_e(\text{O III}), \text{K}$	20900±500	19200±400	19000±400	19400±400	17200±300
$T_e(\text{O II}), \text{K}$	15600±300	15500±300	15500±300	15600±300	15000±300
$T_e(\text{Ar III}), \text{K}$	18800±400	17700±300	17900±300	18100±400	15900±300
$N_e(\text{S II}), \text{cm}^{-3}$	640±170	470±110	620±140	260±100	190± 80
$\text{O}^+/\text{H}^+ \times 10^5$	0.138±0.009	0.239±0.014	0.160±0.010	0.201±0.016	0.155±0.009
$\text{O}^{2+}/\text{H}^+ \times 10^5$	3.304±0.190	4.154±0.226	2.631±0.144	3.434±0.195	5.836±0.304
$\text{O}^{3+}/\text{H}^+ \times 10^6$	0.598±0.051	0.545±0.043	0.943±0.066	0.588±0.053	1.393±0.104
$\text{O}/\text{H} \times 10^5$	3.502±0.190	4.448±0.227	2.886±0.145	3.697±0.196	6.131±0.304
$12+\log(\text{O}/\text{H})$	7.544±0.024	7.648±0.022	7.460±0.022	7.567±0.023	7.788±0.022
$\text{N}^+/\text{H}^+ \times 10^6$	0.087±0.005	0.087±0.004	0.320±0.014	0.064±0.003	0.076±0.003
$ICF(\text{N})$	22.32	16.43	16.06	16.34	33.36
$\text{N}/\text{H} \times 10^6$	1.952±0.115	1.430±0.073	5.139±0.245	1.049±0.062	2.546±0.132
$\log(\text{N}/\text{O})$	-1.254±0.035	-1.493±0.031	-0.749±0.030	-1.547±0.035	-1.382±0.031
$\text{Ne}^{2+}/\text{H}^+ \times 10^5$	0.649±0.037	0.751±0.042	0.345±0.020	0.674±0.040	1.102±0.061
$ICF(\text{Ne})$	1.02	1.02	1.04	1.03	1.00
$\text{Ne}/\text{H} \times 10^5$	0.664±0.040	0.769±0.045	0.358±0.021	0.694±0.043	1.107±0.064
$\log(\text{Ne}/\text{O})$	-0.722±0.035	-0.762±0.034	-0.907±0.033	-0.726±0.036	-0.743±0.033
$\text{S}^+/\text{H}^+ \times 10^6$	0.027±0.001	0.040±0.002	0.026±0.001	0.039±0.002	0.037±0.001
$\text{S}^{2+}/\text{H}^+ \times 10^6$	0.171±0.014	0.250±0.016	0.152±0.011	0.285±0.019	0.379±0.022
$ICF(\text{S})$	2.86	2.06	2.64	2.18	3.91
$\text{S}/\text{H} \times 10^6$	0.567±0.041	0.600±0.033	0.470±0.029	0.704±0.042	1.625±0.088
$\log(\text{S}/\text{O})$	-1.791±0.040	-1.870±0.032	-1.788±0.034	-1.720±0.035	-1.577±0.032
$\text{Cl}^{2+}/\text{H}^+ \times 10^8$...	0.560±0.072
$ICF(\text{Cl})$...	1.52
$\text{Cl}/\text{H} \times 10^8$...	0.853±0.110
$\log(\text{Cl}/\text{O})$...	-3.718±0.060
$\text{Ar}^{2+}/\text{H}^+ \times 10^7$	0.513±0.022	0.781±0.031	0.309±0.176	0.828±0.033	1.116±0.044
$ICF(\text{Ar})$	2.14	1.79	1.77	1.79	2.78
$\text{Ar}/\text{H} \times 10^7$	1.098±0.191	1.396±0.128	0.546±0.078	1.479±0.185	3.101±0.353
$\log(\text{Ar}/\text{O})$	-2.504±0.079	-2.503±0.046	-2.723±0.066	-2.398±0.062	-2.296±0.054
[Fe III] $\lambda 4658$:					
$\text{Fe}^{2+}/\text{H}^+ \times 10^6$...	0.066±0.009	0.102±0.010	...	0.054±0.007
$ICF(\text{Fe})$...	25.01	24.64	...	51.77
$\text{Fe}/\text{H} \times 10^6$...	1.662±0.235	2.516±0.247	...	2.780±0.354
$\log(\text{Fe}/\text{O})$...	-1.428±0.065	-1.059±0.048	...	-1.344±0.060
[O/Fe]	...	0.158±0.065	-0.211±0.048	...	0.073±0.060
[Fe III] $\lambda 4988$:					
$\text{Fe}^{2+}/\text{H}^+ \times 10^6$...	0.100±0.009
$ICF(\text{Fe})$...	25.01
$\text{Fe}/\text{H} \times 10^6$...	2.495±0.236
$\log(\text{Fe}/\text{O})$...	-1.251±0.047
[O/Fe]	...	-0.169±0.047

+ $\lambda 5007$) ratio. To take into account the electron temperatures for different ions, we have used the expressions of Izotov et al. (2006). The electron number density $N_e(\text{S II})$ is derived from the $[\text{S II}] \lambda 6717/\lambda 6731$ emission line ratio. However, we were not able to derive the electron number density from the $[\text{O II}] \lambda 3726, 3729$ doublet because of insufficient spectral resolution.

The electron temperatures $T_e(\text{O III})$ in the studied CS-FGs are high (Table 5), ranging from $\sim 17000\text{K}$ to $\sim 21000\text{K}$. The electron number density $N_e(\text{S II})$, characteristic of the

low-ionization zone of the H II region, is also relatively high. It ranges from 470 cm^{-3} to 640 cm^{-3} in J0159+0751, J1032+4919 and J1205+4551 and is somewhat lower, 190 cm^{-3} and 260 cm^{-3} in J1355+4651 and J1608+3528, respectively. This is to be compared with average values of $\leq 100 \text{ cm}^{-3}$ generally found for H II regions in SFGs. Thus, the H II regions in the selected galaxies with extreme O_{32} are hot and dense.

Ionic and total heavy element abundances are presented in Table 5, together with the ionization correction

factors ICF for unseen stages of ionization. The derived oxygen abundances are low, ranging from $12+\log O/H = 7.46$ to 7.79 . These values are lower than those derived by Izotov et al. (2016a,b) for the $z \sim 0.3$ LyC leaking galaxies (between 7.8 and 8.0). The other heavy element to oxygen abundance ratios are shown in Fig. 4. Except for nitrogen (Fig. 4a), the abundance ratios for the CSFGs studied in this paper (filled stars) are similar to those derived for a sample of BCDs with high signal-to-noise ratio spectra (Izotov et al. 2006) shown by dots in Fig. 4. We note however that the Ar/O ratio for the galaxy J1205+4551 (the most metal-poor object in Fig. 4e) may somewhat be underestimated. This is because the Ar abundance is determined from the [Ar III] $\lambda 7135\text{\AA}$ emission line, which is redshifted to the wavelength $\sim \lambda 7600\text{\AA}$ where the telluric absorption is strong. Although we corrected the galaxy spectrum for this effect using a standard star spectrum, one should keep in mind that the spectrum of the standard star has a worse spectral resolution, having been obtained with a 5 arcsec wide slit, while the galaxy was observed with a considerably narrower 1.2 arcsec wide slit.

The only element which shows a large dispersion is nitrogen (Fig. 4a). While the three highest-metallicity objects in our sample have N/O abundance ratios similar to those obtained for the BCD sample, a higher N/O abundance ratio is found for the two lowest-metallicity galaxies. The most extreme case is the galaxy J1205+4551, with a N/O ratio ~ 0.8 dex higher than the average value for BCDs at that metallicity. Such a large difference cannot be explained by the nitrogen enrichment of an uniform H II region, with a constant electron number density (Izotov et al. 2006). This is however possible in inhomogeneous H II regions with, for example, dense clumps enriched in nitrogen around massive stars with stellar winds. In this case, nitrogen emission lines would be enhanced because of both higher nitrogen abundances and higher electron number densities in clumps, while oxygen lines would only be enhanced by the latter. Therefore, in such H II regions, the enhanced N/O abundance ratio is not characteristic of the entire H II region, but mostly of nitrogen-enriched clumps.

5 BROAD $H\alpha$ LINE EMISSION

One of the most interesting features of the CSFG spectra with extreme O_{32} is the presence of a low-intensity broad component of the $H\alpha$ emission line in all of them (see insets in Fig. 3). These broad components with intensities $\sim 1 - 10$ percent that of the $H\alpha$ line are seen in a minority of SFG spectra (Izotov, Thuan & Guseva 2007). They imply the presence in these galaxies of rapid dynamical processes, either expanding envelopes of massive stars with stellar winds or supernova remnants in their early stage of expansion. Our spectra do not show the presence of broad blue ($\sim \lambda 4650\text{\AA}$) or red ($\sim \lambda 5800\text{\AA}$) bumps, characteristic of Wolf-Rayet stars (see insets in Fig. 3), thus ruling out the hypothesis of massive stars with stellar winds. Therefore, the most likely mechanism for broad $H\alpha$ emission appears to be expanding young supernova remnants in the early stages of their evolution.

In Fig. 5 we present for all five CSFGs the spectral region around the $H\alpha$ emission line, with the Gaussian fit to

the broad component. The flux ratios of broad-to-total $H\alpha$ emission and the full widths at half maximum (FWHM) in km s^{-1} of the broad emission are shown in Table 6. We see that the fraction of broad emission is small (< 3 percent), but that expansion velocities are high, with FWHMs ranging from ~ 1700 to $\sim 2000 \text{ km s}^{-1}$. Such rapid ionized gas motions may facilitate escape of the resonant Ly α emission from the galaxy. They should be taken into account in models of its transfer through the H II region.

6 O_{32} AND HELIUM LINE INTENSITIES AS DIAGNOSTICS FOR LYMAN CONTINUUM LEAKAGE IN CSFGS

One of the important questions of contemporary cosmology is whether SFGs can lose their ionizing radiation and, if so, in which quantities. The answer to that question has direct consequences on the problem of the reionization of the Universe. It has been suggested that dwarf SFGs at redshifts 5 – 10 can be the main contributors of the intergalactic medium ionization, if the escape fraction of their ionizing radiation is $\gtrsim 10$ percent (Ouchi et al. 2009; Robertson et al. 2013, 2015). Such galaxies could have large O_{32} because of their low column densities of neutral gas. However, O_{32} depends also on metallicity, the starburst age, and the ionization parameter which is higher in denser, compact, and more luminous SFGs. Because of these other dependences, Stasińska et al. (2015) have concluded from various emission-line diagnostic diagrams that the escape fraction from photoionized H II regions cannot exceed 10 percent, even with the highest observed O_{32} . If shocks are present, they can enhance the [O II] $\lambda 3727\text{\AA}$ emission line, reducing O_{32} as compared to the value expected for a density-bounded photoionized H II region (Jaskot & Oey 2013; Stasińska et al. 2015).

Therefore, other diagnostics in the optical range are needed which are based not only on O_{32} . We propose to use the He I emission lines, that are sensitive to the electron number density and the optical depth, to find density-bounded H II regions. Helium emission, in contrast to the collisionally excited oxygen lines, is mainly produced via recombination. However, in the presence of a significant electron number density and a large optical depth in some He I emission lines, there can also be contributions from collisional excitation and fluorescent enhancement processes. By examining the intensity ratios of several He I emission lines, we are able to constrain both the electron number density and the optical depth in the H II region.

In the optical range, the optimal set of He I emission lines for constraining those two quantities consists of a set of three lines: the $\lambda 3889\text{\AA}$, $\lambda 6678\text{\AA}$ and $\lambda 7065\text{\AA}$ lines. All three lines are sensitive to collisional excitation, with the most sensitive one being the He I $\lambda 7065\text{\AA}$ line (Benjamin, Skillman & Smits 1999, 2002; Izotov, Stasińska & Guseva 2013). Additionally, the He I $\lambda 3889\text{\AA}$ and $\lambda 7065\text{\AA}$ emission lines are also sensitive to fluorescent enhancement. However, the He I $\lambda 6678\text{\AA}$ emission line intensity is nearly insensitive to this effect. While collisional excitation enhances all lines, the effect of optical depth is different. Thus, a non-negligible optical depth of the He I $\lambda 3889\text{\AA}$ transition decreases its intensity. The problem, how-

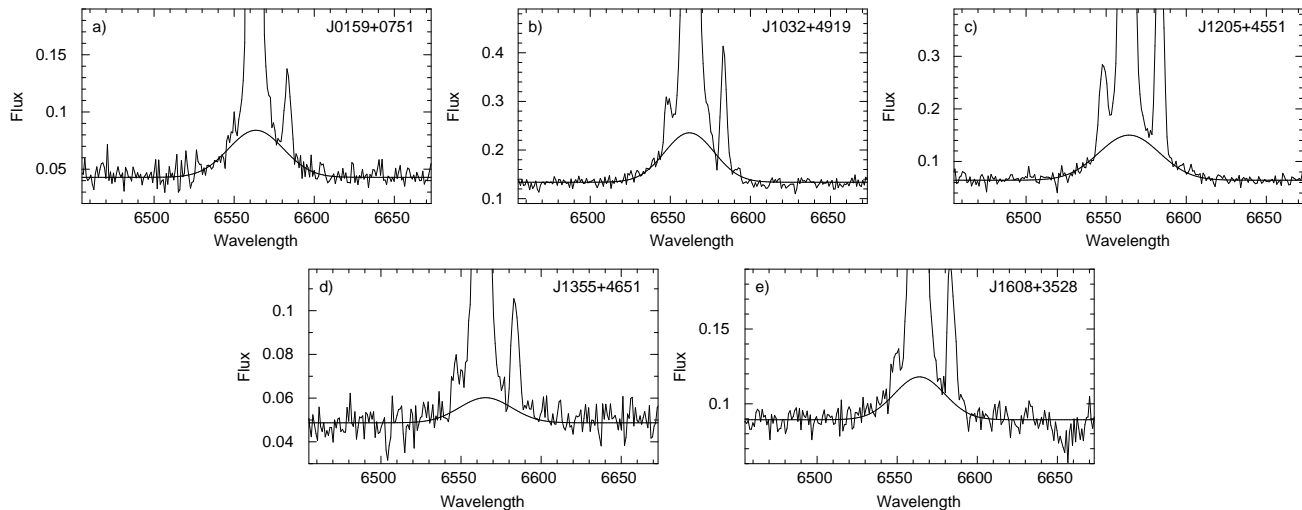


Figure 5. The observed H α profiles with fits of their broad components.

Table 6. Broad H α emission

Name	$F(\text{broad})/F(\text{total})$ (%)	FWHM (km s $^{-1}$)
J0159+0751	1.9	1850
J1032+4919	1.4	1670
J1205+4551	2.6	2040
J1355+4651	0.5	1750
J1608+3528	0.7	1680

ever, with this line is that it is blended with the hydrogen H δ λ 3889Å emission line. Therefore, we have subtracted the hydrogen line from the blend, adopting its intensity to be equal to 0.107 that of the H β emission line for the electron temperature $T_e = 15000 - 20000\text{K}$ (Storey & Hummer 1995). As for the He I λ 7065Å emission line, its intensity is strongly increased because of both collisional excitation and fluorescence. It is seen in Fig. 3 that the He I λ 7065 line in J0159+0751, J1032+4919 and J1205+4551 is much stronger than the He I λ 6678 line, indicating higher densities and/or optical depths in these galaxies. On the other hand, in J1355+4651 and J1608+3528, these two lines are comparable in strength, implying lower $N_e(\text{He I})$ and/or optical depths.

Izotov, Thuan & Guseva (2014b) have shown that the electron number density $N_e(\text{He I})$ is correlated with $N_e(\text{S II})$ in high-excitation H II regions, although in relatively dense regions, $N_e(\text{He I})$ is somewhat larger than $N_e(\text{S II})$. Since $N_e(\text{He I})$ is a characteristic of the entire H II region, while $N_e(\text{S II})$ is related only to its outer zone and the photodissociation region (PDR) around it, we may conclude that the central part of the H II region is denser than its outer part. In this paper, we use the He I λ 3889/ λ 6678 and λ 7065/ λ 6678 flux ratios, which depend on both the $N_e(\text{He I})$ and $\tau(\text{He I } \lambda$ 3889), to check whether this conclusion holds for our five CSFGs as well. For this, we adopt the analytical approximations of the He I line fluxes by Izotov et al. (2013), based on the He I emissivities of Porter et al. (2012, 2013). These approximations depend on three parameters, the electron temperature, the electron number density $N_e(\text{He I})$ and the op-

tical depth $\tau(\text{He I } \lambda$ 3889). For the electron temperature, we adopt $T_e(\text{O III})$ (Table 5), while $N_e(\text{He I})$ and $\tau(\text{He I } \lambda$ 3889) are derived from the extinction-corrected He I λ 3889/ λ 6678 and λ 7065/ λ 6678 flux ratios (Table 4).

The results of our calculations are shown in Table 7, where we present the derived $N_e(\text{He I})$ and $\tau(\text{He I } \lambda$ 3889) and compare the observed and calculated He I λ 3889/ λ 6678 and λ 7065/ λ 6678 flux ratios, together with the low-density case B ratios. By comparing $N_e(\text{He I})$ in Table 7 with $N_e(\text{S II})$ in Table 5, we find that $N_e(\text{He I})$ is, in four out of five CSFGs, higher than $N_e(\text{S II})$, and in one object, J1205+4551, they are comparable. This confirms the result of Izotov et al. (2014b) that, on average, $N_e(\text{He I})$ is higher than $N_e(\text{S II})$ in H II regions. Furthermore, in the three CSFGs with a strong He I λ 7065 line, J0159+0751, J1032+4919 and J1205+4551, the electron number density and optical depth are considerably higher than in the remaining two galaxies, J1355+4651 and J1608+3528. Since, according to photoionization models of H II regions, $\tau(\text{He I } \lambda$ 3889) increases with increasing column density of the neutral gas, we conclude that the former three galaxies are more optically thick to the LyC radiation than the two later ones, although the optical depth in J0159+0751 is considerably smaller than those in J1032+4919 and J1205+4551 (Table 7).

We further produce a grid of photoionized H II region models using the CLOUDY code c13.04 (Ferland et al. 1998, 2013) with fixed neutral hydrogen column densities $N(\text{H I})$, ranging from 10^{17} to 10^{19} cm $^{-2}$, with the lowest and highest values corresponding to two limiting cases of the optical

Table 7. He I emission-line ratios, electron density $N_e(\text{He I})$ and optical depth $\tau(3889)$

Name	$N_e(\text{He I})$ (cm^{-3})	$\tau(\text{He I } \lambda 3889)$	$I(\text{He I } \lambda 3889)/I(\text{He I } \lambda 6678)$			$I(\text{He I } \lambda 7065)/I(\text{He I } \lambda 6678)$		
			obs.	cal.	low-density case B	obs.	cal.	low-density case B
J0159+0751	2246	0.8	2.86	2.79	3.91	2.47	2.47	0.92
J1032+4919	695	7.2	2.04	2.04	3.78	2.39	2.39	0.87
J1205+4551	595	10.5	1.48	1.48	3.76	2.70	2.70	0.87
J1355+4651	314	0.0	3.39	3.51	3.80	0.74	1.01	0.88
J1608+3528	399	0.0	3.49	3.42	3.61	1.07	0.98	0.82

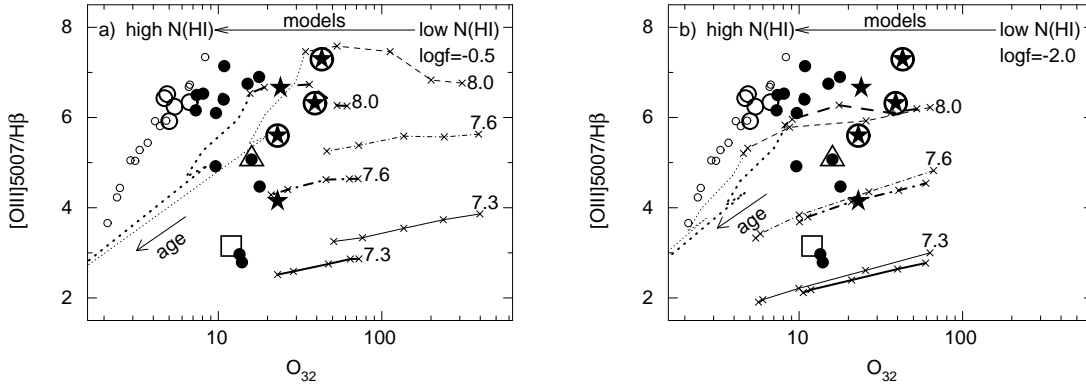


Figure 6. The $[\text{O III}]5007/\text{H}\beta - O_{32}$ diagram for a) $\log f = -0.5$ and b) $\log f = -2.0$. The five CSFGs with extremely high O_{32} studied here are shown by filled stars. The encircled filled stars correspond to CFSGs with small neutral hydrogen column densities $N(\text{H I})$, as predicted from He I line ratios, while the non-encircled stars correspond to those with high $N(\text{H I})$. The five low- z LyC leakers studied by Izotov et al. (2016a,b) are shown by large open circles. The BCDs SBS 0335–052 with a Ly α line in absorption, and Tol 1214–277 with a prominent Ly α emission line (Thuan & Izotov 1997), are shown by an open square and an open triangle, respectively. A sample of BCDs with $O_{32} \sim 5 - 20$, observed with the LBT (Izotov et al., 2017, in preparation) is represented by filled circles, while confirmed Ly α emitting galaxies (Yang et al. 2017) are shown by small open circles. CLOUDY models for a burst with the age of 2 Myr and fixed ionization parameters with three values of the oxygen abundance $12+\log\text{O}/\text{H} = 7.3, 7.6$ and 8.0 are shown by solid, dash-dotted and dashed lines, respectively, and those with two values of the electron number density $N_e = 100$ and 1000 cm^{-3} are represented by thin and thick lines, respectively. Crosses on the modelled lines correspond to $N(\text{H I})$ ranging from 10^{17} cm^{-2} to 10^{19} cm^{-2} , in steps of 0.5 dex and increasing from right to left. The dotted lines show the evolutionary sequences calculated for CLOUDY optically thick models adopting $N_e = 1000 \text{ cm}^{-3}$ (thick dotted line) and $N_e = 100 \text{ cm}^{-3}$ (thin dotted line) with $12+\log\text{O}/\text{H} = 8.0$ and starburst ages varying from 1 Myr to 6 Myr. The age direction is given by the arrow.

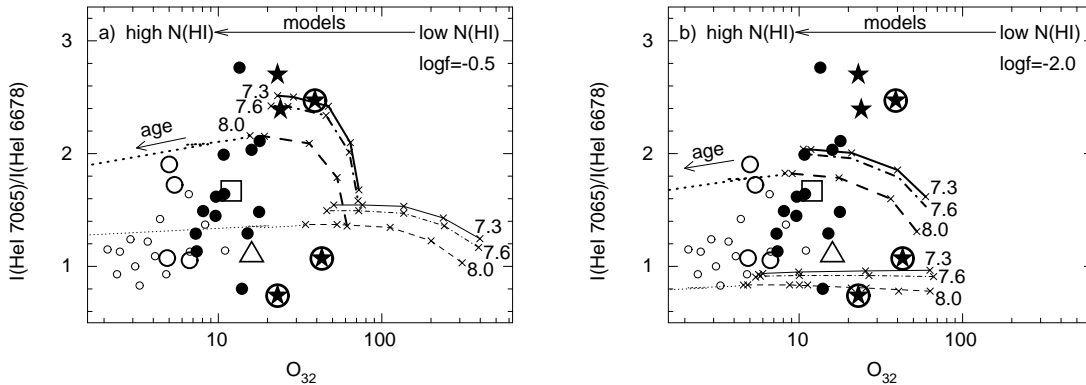


Figure 7. The $I(\text{He I } \lambda 7065)/I(\text{He I } \lambda 6678) - O_{32}$ diagram for a) $\log f = -0.5$ and b) $\log f = -2.0$. Symbols and lines are the same as in Fig. 6. The LyC leaker J1333+6246 with noisy He I $\lambda 6678$ and $\lambda 7065$ lines in its SDSS spectrum is not shown.

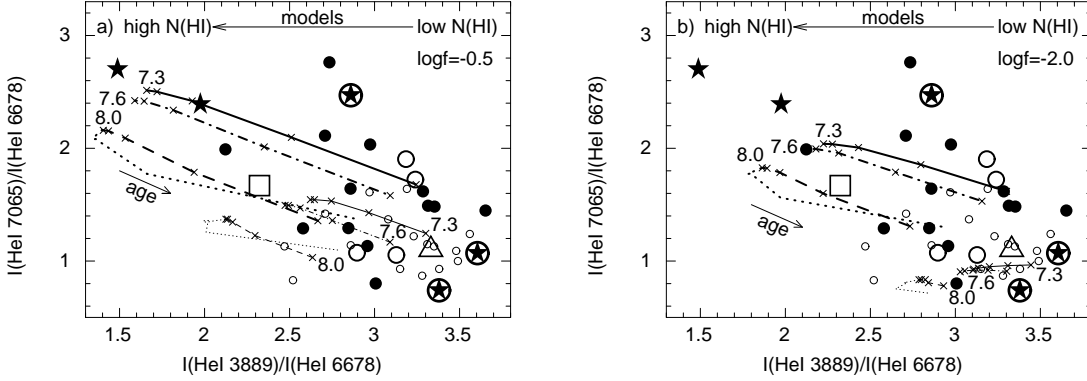


Figure 8. The $I(\text{He I } \lambda 7065)/I(\text{He I } \lambda 6678) - I(\text{He I } \lambda 3889)/I(\text{He I } \lambda 6678)$ diagram for (a) $\log f = -0.5$ and (b) $\log f = -2.0$. Symbols and lines are the same as in Fig. 6. The LyC leaker J1333+6246 (Izotov et al. 2016b) with noisy He I $\lambda 6678$ and $\lambda 7065$ lines in its SDSS spectrum is not shown.

depth: a low optical depth of ~ 0.7 in the Lyman continuum and a high escape fraction $f_{\text{esc}}^{\text{LyC}} \gtrsim 20$ percent, and a high optical depth of ~ 70 in the Lyman continuum and a negligible LyC escape fraction.

It has empirically been found from *HST* observations that the escape fraction $f_{\text{esc}}^{\text{LyC}}$ of ionizing radiation in low- z leakers increases with increasing O_{32} (Izotov et al. 2016b). We wish here to investigate whether this empirical relation can also be predicted by photoionized H II region models, i.e. are high modelled O_{32} ratios reliable indicators of the escaping LyC radiation? Similar studies have been conducted by Jaskot & Oey (2013), Nakajima & Ouchi (2014) and Stasińska et al. (2015), with somewhat contradictory and inconclusive results. Stasińska et al. (2015) used various emission-line diagnostics of a large sample of BCDs from the SDSS and found that their properties can be fully explained by ionization-bounded H II region models with a low LyC escape fraction, including galaxies with the highest O_{32} , if the ionizing radiation flux is purely of stellar origin. On the other hand, Jaskot & Oey (2013) and Nakajima & Ouchi (2014) suggested that high O_{32} may be a good indicator of escaping LyC radiation. However, although some models of Nakajima & Ouchi (2014) do predict higher O_{32} at higher $f_{\text{esc}}^{\text{LyC}}$, they also have models that allow escaping LyC radiation with any O_{32} . Furthermore, modelled O_{32} ratios in high- z Ly α emitting galaxies are a factor $\sim 2-5$ too high for their ionization parameters (see fig. 11 in Nakajima & Ouchi 2014). Thus, by itself, the modelled O_{32} is a poor indicator of $f_{\text{esc}}(\text{LyC})$. It should be combined with some observational data, such as metallicity, various emission-line flux ratios, and the $H\beta$ equivalent width $\text{EW}(H\beta)$ which is related to the starburst age and hence to the hardness of the ionizing radiation. Used together, these data would better constrain the physical conditions in the H II region.

The modelled O_{32} ratio at a fixed ionization parameter can be decreased to better fit observed ratios if other sources of ionizing radiation, e.g. radiative shocks, are considered (Jaskot & Oey 2013; Stasińska et al. 2015). Unfortunately, in its present state, the CLOUDY code does not include self-consistently both the stellar radiation and the radiation from radiative shocks. Furthermore, the fast radiative shock models in existence consider only shocks propagating through the neutral gas (Allen et al. 2008), while

in CSFGs, shocks are also likely to propagate through the ionized medium. Additionally, the modelled O_{32} ratio for a fixed ionization parameter decreases when the starburst age increases (Jaskot & Oey 2013).

Keeping in mind all these caveats, we have generated a grid of CLOUDY models to check the reliability of the modelled O_{32} ratio as an indicator of LyC leakage. There are many input parameters in the CLOUDY models. Some of the parameters can be obtained directly from observations. The chemical composition can be derived from the emission-line intensities in the galaxy spectrum. The rate of ionizing photon production Q and the shape of the ionizing radiation spectrum are determined from the $H\beta$ luminosity and the starburst age. The latter quantity can be derived, for an instantaneous burst, from the $H\beta$ equivalent width $\text{EW}(H\beta)$. The electron number density N_e is derived from the observed intensities of $[\text{S II}]\lambda 6717, 6731$ or from the He I emission lines. The determination of other input parameters, for instance, the inner radius of the H II region, the turbulent velocity, and the filling factor f , is more complicated. They can be derived by comparing the observed and modelled emission-line intensities for each galaxy.

Our aim here is to study general statistical trends of the galaxy sample. Therefore, we have calculated a grid of models for three different values of the oxygen abundance, $12+\log O/H = 7.3, 7.6$ and 8.0 , and a fixed ionization parameter. For elements heavier than helium, we have adopted their abundances relative to that of oxygen to be the abundance ratios given by Izotov & Thuan (1999) and Izotov et al. (2006). The helium abundance is chosen from the relation between the helium mass fraction and oxygen abundance of Izotov et al. (2014b). We also included dust with Orion-like properties, provided by the CLOUDY code, and scaling it according to the oxygen abundance. We adopt $Q = 10^{53} \text{ s}^{-1}$, which corresponds to the average observed $H\beta$ luminosity in our galaxies, and a shape of the ionizing radiation spectrum corresponding to the Starburst99 model with an age of 2.0 Myr. For the inner radius of the H II region, we have adopted the value $R_{\text{in}} = 50 \text{ pc}$. Reducing R_{in} by a factor of 10 would result in increasing O_{32} by a factor of up to ~ 1.5 in models with $N(\text{H I}) \lesssim 10^{18} \text{ cm}^{-2}$, but the He I flux ratios would be changed by not more than 10 percent in models with any $N(\text{H I})$. The models were calculated for

two values of the filling factor f with $\log f = -0.5$ and -2.0 and two electron number densities $N_e = 100$ and 1000 cm^{-3} . We also set the turbulent velocity to 0.

To investigate the effect of the hardness of the ionizing radiation at a given metallicity, we have calculated additionally, for an oxygen abundance $12+\log O/H = 8.0$, a set of models with starburst ages in the range 1 – 6 Myr, characterized by an equivalent width $EW(H\beta)$ in the range $\sim 50 - 500 \text{ \AA}$ (thick dotted lines for $N_e = 1000 \text{ cm}^{-3}$ and thin dotted lines for $N_e = 100 \text{ cm}^{-3}$ in Fig. 8). The other parameters remained the same.

We wish to find the models which fit simultaneously the $[O \text{ III}]\lambda 5007/H\beta$ emission-line ratio, the O_{32} ratio, and the He I line ratios. The results of our model calculations and their comparison with the data are shown in Figs. 6–8. The diagrams $[O \text{ III}]\lambda 5007/H\beta - O_{32}$ and $\lambda 7065/\lambda 6678 - O_{32}$ for models with $\log f = -0.5$ and $\log f = -2.0$, corresponding to the logarithm of the ionization parameter in the range $\sim -1.5 - -2.5$, are presented in Figs. 6a – 6b and Figs. 7a – 7b, respectively. We note that, for a given metallicity and a given electron number density, the $[O \text{ III}]\lambda 5007/H\beta$ ratio changes only slowly with $N(H \text{ I})$, while O_{32} undergoes large variations. It is seen that the location of all extreme CSFGs (filled stars) can be explained by models with $\log f = -0.5$ and high $N(H \text{ I})$ (Fig. 6a and 7a). Alternatively, models with much lower filling factors ($\log f = -2.0$), and correspondingly, with lower ionization parameters, are needed to fit observations with lower modelled $N(H \text{ I})$ (Fig. 6b and 7b). However, in the latter case, the models are unable to reproduce the observed $[O \text{ III}]\lambda 5007/H\beta$ ratios (Fig. 6b), predicting too low values for the galaxy metallicities (Table 5). Furthermore, the models fail to reproduce the observed line intensity ratios for three out of the five extreme CSFGs in Fig. 7b. Therefore, we conclude that the models with low $\log f = -2.0$, and hence with low ionization parameters, are not likely good fits to our extreme CSFGs.

For comparison, we have also plotted other data sets in those Figures. The first set consists of the LyC leakers studied by Izotov et al. (2016a,b) (large open circles). We find that, in Figs. 6 – 7, these objects lie in the region corresponding to high $N(H \text{ I})$, irrespective of the value of $\log f$, in apparent disagreement with the relatively high LyC escape fraction observed for these objects. Similarly to the extreme CSFGs, the $[O \text{ III}]\lambda 5007/H\beta$ ratios of ~ 6 in the LyC leakers with oxygen abundances 7.8 – 8.0 are well reproduced by models with $\log f = -0.5$ while models with $f = -2.0$ predict too low values. The second data set shown (filled circles) consists of a sample of high-excitation CSFGs with $O_{32} \sim 5 - 20$ and oxygen abundances in the range $\sim 7.3 - 7.8$, observed with the LBT (Izotov et al. 2017, in preparation). The range of the $\lambda 7065/\lambda 6678$ ratios of the galaxies in the second set is similar to that of CSFGs with extremely high O_{32} . The galaxies are also located in the region corresponding to models with high $N(H \text{ I})$. The third set includes Ly α emitting GPs observed with the *HST*/COS (small open circles, Yang et al. 2017). These objects, with oxygen abundances of ~ 8.0 , are characterized by O_{32} ratios in the lowest range, $\sim 2 - 10$, and they are the most deviant from model predictions. They also have lower $[O \text{ III}]\lambda 5007/H\beta$ ratios and lower $H\beta$ equivalent widths $EW(H\beta)$, indicating higher burst ages compared to extreme CSFGs and LyC leakers.

To investigate the effects of age and hence varying the

hardness of ionizing radiation we show by dotted lines in Fig. 6 the dependences for optically thick models with a fixed oxygen abundance of 8.0, and N_e of 1000 cm^{-3} (thick dotted line) and of 100 cm^{-3} (thin dotted line), and starburst ages varying from 1 Myr to 6 Myr in the direction shown by the arrow. These models indicate that O_{32} strongly depends not only on the ionization parameter, but also on the hardness of the ionizing radiation. The range of predicted $[O \text{ III}]\lambda 5007/H\beta$ ratios is sufficiently large, extending down to < 3 for starburst ages ≥ 5 Myr, to account for the observed values. However, the modelled values of O_{32} remain too high for a fixed $[O \text{ III}]\lambda 5007/H\beta$ ratio, and the models indicate high $N(H \text{ I})$ for the Ly α emitting GPs.

In Fig. 7, the modelled O_{32} span a large range of values (dotted lines) and can reproduce the observed O_{32} in the Ly α emitting GPs (small open circles, Yang et al. 2017). However, the lowest O_{32} (< 1) correspond to large starburst ages (≥ 5 Myr) and thus to low $EW(H\beta)$ ($< 100 \text{ \AA}$). This is inconsistent with the high $EW(H\beta)$ ($> 100 \text{ \AA}$) and $O_{32}(\geq 2)$, observed by Yang et al. (2017) in most of the Ly α emitting GPs.

Finally, we show respectively by an open square and an open triangle in Figs. 6 – 7 the BCDs SBS 0335–052 with the oxygen abundance of ~ 7.3 (Izotov et al. 2009) and Tol 1214–277 with the oxygen abundance of ~ 7.5 (Izotov, Chaffee & Green 2001). Their $[O \text{ III}]\lambda 5007/H\beta$ ratios are well reproduced by the models with $\log f = -0.5$ (Fig. 6a). These two objects have been observed by Thuan & Izotov (1997) in the UV range with the *HST*. The Ly α line in the UV spectrum of SBS 0335–052 is in absorption. The neutral hydrogen column density derived from the line profile is very high, $7 \times 10^{21} \text{ cm}^{-2}$ (Thuan & Izotov 1997), implying a very low LyC escape fraction. On the other hand, strong Ly α emission is detected in the UV spectrum of Tol 1214–277, suggesting a high LyC escape fraction. Yet, in spite of that difference, both galaxies with the electron number densities $N_e \sim 200 \text{ cm}^{-3}$ in their H II regions are characterised by similar $O_{32} \sim 15$ (Izotov et al. 2001, 2009).

The above discussion implies that O_{32} derived from photoionized H II region models are in general too high compared to the observed ones for a fixed ionization parameter and metallicity. Thus it cannot be a sure indicator of escaping Ly α radiation, nor can it indicate escaping LyC radiation and density-bounded H II regions with certainty. The possible reason for the disagreement between modelled and observed O_{32} could be due to the fact that the models include only ionizing radiation from stars. If additional sources of gas ionization and heating are included in the model, e.g. radiative shocks producing extreme UV radiation or sources producing X-ray emission, then O_{32} would be changed. Furthermore, we have considered only homogeneous H II region models with a constant N_e , although density inhomogeneities may play a role.

More definite conclusions about LyC leakage can however be drawn from the He I emission-line flux ratios. Fig. 8 shows the $\lambda 7065/\lambda 6678 - \lambda 3889/\lambda 6678$ diagram, where we display the modelled relations between these line ratios for two values of the electron number density and for three values of the oxygen abundance. There is a clear dependence of the relations on metallicity caused presumably by varying electron temperatures in H II regions, the temperatures being higher for lower metallicities. The He I $\lambda 7065/\lambda 6678$

ratio also increases with increasing N_e because the $\lambda 7065$ transition is much more sensitive to collisional enhancement compared to the $\lambda 6678$ transition. On the other hand, the $\lambda 3889$ transition is less sensitive to collisional enhancement compared to the $\lambda 6678$ transition, therefore the He I $\lambda 3889/\lambda 6678$ ratio decreases with increasing N_e .

The locations of the two out of three extreme CSFGs (non-encircled stars) with the highest $\lambda 7065/\lambda 6678$ ratios correspond to high column densities ($N(\text{H I}) \gtrsim 10^{19} \text{ cm}^{-2}$). On the other hand, the three remaining CSFGs (encircled stars) are located in the region corresponding to low column densities ($N(\text{H I}) \lesssim 10^{17.5} \text{ cm}^{-2}$). This implies that the LyC escape fractions in these three galaxies may be high and that follow-up Ly α observations may be warranted.

It is interesting that the locations of the four LyC leakers at $z \sim 0.3$ in Fig. 8a (large open circles) and of the Ly α emitting GPs (small open circles) are consistent with the low $N(\text{H I})$ predicted by the models with high $\log f$. The $N(\text{H I})$ for the Ly α emitting GPs are predicted to be lower than 10^{19} cm^{-2} . However, we note that the He I $\lambda 6678\text{\AA}$ and $\lambda 7065\text{\AA}$ line fluxes in LyC leakers measured from the SDSS spectra are somewhat uncertain because of their faintness and their location in a wavelength range that contains numerous residuals of night sky emission lines. Our results are somewhat contradictory with the higher neutral hydrogen column densities derived by Yang et al. (2017), using radiative transfer models for the Ly α line in the Ly α emitting GPs. Those authors derived column densities $N(\text{H I})$ in the range $10^{16} - 10^{20.6} \text{ cm}^{-2}$, with an average value of more than 10^{19} cm^{-2} . Their sample includes the five LyC leakers of Izotov et al. (2016a,b). For one LyC leaker, J1503+3644, Yang et al. (2017) derived a low $N(\text{H I}) = 10^{16.8} \text{ cm}^{-2}$, but the best fit of $N(\text{H I})$ for the remaining LyC leakers is $\gtrsim 10^{19} \text{ cm}^{-2}$, larger than the value that permits LyC escape. Therefore, Yang et al. (2017) suggested that LyC emission in these galaxies probably escapes through holes in the interstellar medium with much lower $N(\text{H I})$.

As for the objects in the sample of CSFGs with $O_{32} \sim 5 - 20$ observed with the LBT (filled circles), they are distributed in a region spanning a broad range of $\lambda 3889/\lambda 6678$ and $\lambda 7065/\lambda 6678$ line ratios, with a significant fraction of the galaxies characterized by low $N(\text{H I})$ (Fig. 8a), despite the fact that H II regions with high $\lambda 7065/\lambda 6678$ line ratios in some of these galaxies are very dense. It is also interesting to note that the BCD SBS 0335–052 with its Ly α line in absorption is characterized, as expected, by a high $N(\text{H I})$, while the BCD Tol 1214–277 with its Ly α line in emission is characterized by a low $N(\text{H I})$.

Somewhat different conclusions are drawn if we compare the observations with models characterized by a low $\log f = -2.0$. High $N(\text{H I})$ are predicted for many galaxies, including two LyC leakers, if a low electron number density N_e is adopted. In this case, the observed $[\text{O III}]\lambda 5007/\text{H}\beta$ ratios are higher than those predicted by the models (Fig. 6b). Furthermore, the observed electron number densities $N_e(\text{S II})$ of most LyC leakers (Izotov et al. 2016a,b) and of many Ly α emitting GPs are several times greater than 100 cm^{-3} , although these values are somewhat uncertain because of large errors. We therefore conclude that the models with a low $\log f = -2.0$ and a low N_e are less likely to fit the data than those with high $\log f = -0.5$ and high N_e . More accurate electron number densities are needed to draw

more definite conclusions on the escaping ionizing radiation in the above galaxies.

To investigate the effect of varying hardness of radiation, we show by dotted lines in Fig. 8 the same optically thick models with various starburst ages, as in Figs. 6 – 7. They reveal an interesting behaviour. For starburst ages < 4 Myr, the He I emission-line ratios depend weakly on starburst age. However, at larger ages, the He I $\lambda 3889/\lambda 6678$ ratio increases with starburst age, while the He I $\lambda 7065/\lambda 6678$ ratio decreases. This behaviour can be understood as a softening of the ionizing radiation, resulting in a decrease of the size of the He⁺ zone and thus in a decrease of the optical depth in the He I $\lambda 3889$ transition. However, all galaxies considered here have a high $\text{EW}(\text{H}\beta)$ and thus a younger burst age, consistent with the case where the He I emission-line ratios vary weakly with starburst age.

Thus, based admittedly on a small sample of galaxies with extreme O_{32} , our investigation has shown that the proposed He I emission flux ratios in the optical range can be useful diagnostics for finding Ly α and LyC leaking galaxies.

7 CONCLUSIONS

In this paper we present Large Binocular Telescope (LBT) spectrophotometric observations of five compact star-forming galaxies (CSFGs) with extremely high $O_{32} = 23 - 43$. CSFGs with such high O_{32} are thought to be good candidates for leaking LyC radiation. As such, their high-redshift counterparts are thought to be the main agents of the reionization of the early Universe. Our goal here is to study the physical conditions and chemical composition of these extreme CSFGs and to investigate whether they can indeed be candidates for LyC leaking galaxies. Our main results are as follows.

1. All spectra show strong emission lines implying the presence of a very young stellar population. This is supported by very high equivalent widths $\text{EW}(\text{H}\beta)$ of the H β emission line with values $370 - 520\text{\AA}$, corresponding to a starburst age < 3 Myr. The electron number densities N_e , derived from the $[\text{S II}]\lambda 6717/\lambda 6731$ flux ratio, are particularly high. They are $190 - 260 \text{ cm}^{-3}$ in two CSFGs and higher, $470 - 640 \text{ cm}^{-3}$, in the three others.

2. A strong $[\text{O III}]\lambda 4363\text{\AA}$ emission line is detected in all objects, allowing element abundance determination by the direct T_e method. We find high electron temperatures $T_e(\text{O III}) \sim 17000 - 21000\text{K}$ and low oxygen abundances $12 + \log \text{O}/\text{H}$ in the range $7.46 - 7.79$. The Ne/O, S/O, Cl/O, Ar/O and Fe/O abundance ratios in all five galaxies are similar to those found in low-metallicity blue compact dwarf (BCD) galaxies. The N/O abundance ratios in three CSFGs are low and also consistent with values found for low-metallicity BCDs. On the other hand, in the two remaining galaxies, the nitrogen abundance is higher by up to 0.8 dex, which is too high to be explained by the chemical enrichment of homogeneous H II regions, with a constant electron number density. Nitrogen-enriched clumps in inhomogeneous H II regions need to be invoked to explain such high N/O abundance ratios.

3. A broad H α emission line is detected in the spectra of all CSFGs, indicating the presence of fast dynamical processes, possibly related to young supernova remnants in

the early stages of their evolution. The full widths at half maximum of the broad component correspond to velocities of $\sim 1800 - 2000 \text{ km s}^{-1}$. Such rapid ionized gas motions may facilitate the escape of the resonant Ly α emission from the galaxy. In one of the CSFGs, J1205+4551, the high-ionization emission line [Ne v] $\lambda 3426\text{\AA}$ is detected, implying the presence of shocks possibly produced by SNe.

4. Various He I emission lines are present in the spectra of the observed CSFGs. We find that the He I $\lambda 7065/\lambda 6678$ flux ratios in three out of five CSFGs are unusually high, indicating high electron number densities $N_e(\text{He I})$ and/or high optical depths $\tau(\lambda 3889)$ in the He I $\lambda 3889$ emission line. This is consistent with the high electron number densities derived from the [S II] emission lines. The He I $\lambda 7065/\lambda 6678$ flux ratios in the remaining two CSFGs are considerably lower, corresponding to a lower $N_e(\text{He I})$ and/or $\tau(\lambda 3889)$.

5. We investigate whether the LyC can leak out of these CSFGs by constraining their neutral gas column density $N(\text{H I})$ through CLOUDY models, using O_{32} and the He I emission-line flux ratios. We find that the modelled O_{32} is not a certain indicator for LyC leakage because it depends also on other parameters, such as the ionization parameter and the hardness of ionizing radiation, the latter depending in turn on the starburst age. Therefore, it alone cannot be used with H II region models for estimation of the neutral gas column density and the LyC escape fraction. The only reliable way for the determination of the $f_{\text{esc}}^{\text{LyC}}$ is to obtain a well-defined empirical relation, based on a large sample, between $f_{\text{esc}}^{\text{LyC}}$ and O_{32} , both derived directly from observations. On the other hand, the modelled He I $\lambda 3889/\lambda 6678$ and $\lambda 7065/\lambda 6678$ emission-line flux ratios are better indicators of possible LyC leakage. We find that in two CSFGs with high $\lambda 7065/\lambda 6678$ flux ratios, the neutral gas column density $N(\text{H I})$ is high, $\gtrsim 10^{19} \text{ cm}^{-2}$, implying a low LyC escape fraction. However, in the three remaining galaxies $N(\text{H I})$ can be below $10^{17.5} \text{ cm}^{-2}$, suggesting that these galaxies can lose a large fraction of their ionizing radiation, up to $\gtrsim 20$ percent.

ACKNOWLEDGEMENTS

Funding for the SDSS-III has been provided by the Alfred P. Sloan Foundation, the Participating Institutions, the National Science Foundation, the U.S. Department of Energy, the National Aeronautics and Space Administration, the Japanese Monbukagakusho, the Max Planck Society, and the Higher Education Funding Council for England. The SDSS Web Site is <http://www.sdss.org/>. GALEX is a NASA mission managed by the Jet Propulsion Laboratory. This research has made use of the NASA/IPAC Extragalactic Database (NED) which is operated by the Jet Propulsion Laboratory, California Institute of Technology, under contract with the National Aeronautics and Space Administration. This publication makes use of data products from the Wide-field Infrared Survey Explorer, which is a joint project of the University of California, Los Angeles, and the Jet Propulsion Laboratory/California Institute of Technology, funded by the National Aeronautics and Space Administration.

REFERENCES

- Alam S. et al., 2015, ApJS, 219, 12
 Allen M. G., Groves B. A., Dopita M. A., Sutherland R. S., Kewley L. J., 2008, ApJS, 178, 20
 Aller L. H., 1984, Physics of Thermal Gaseous Nebulae (Dordrecht: Reidel)
 Baldwin J. A., Phillips M. M., Terlevich R., 1981, PASP, 93, 5
 Benjamin R. A., Skillman E. D., Smits D. P., 1999, ApJ, 514, 307
 Benjamin R. A., Skillman E. D., Smits D. P., 2002, ApJ, 569, 288
 Borthakur S., Heckman T. M., Leitherer C., Overzier R. A., 2014, Science, 346, 216
 Bouwens R. J. et al., 2015, ApJ, 803, 34
 Cardamone C. et al., 2009, MNRAS, 399, 1191
 Cardelli J. A., Clayton G. C., Mathis J. S., 1989, ApJ, 345, 245
 Ferland G. J., Korista K. T., Verner D. A., Ferguson J. W., Kingdon J. B., Verner E. M., 1998, PASP, 110, 761
 Ferland G. J. et al., 2013, Revista Mexicana de Astronomia y Astrofisica, 49, 137
 Girardi L., Bressan A., Bertelli G. Chiosi C., 2000, A&AS, 141, 371
 Izotov Y. I., Thuan T. X., 1999, ApJ, 519, 639
 Izotov Y. I., Chaffee F. H., Green R. F., 2001, ApJ, 562, 727
 Izotov Y. I., Stasińska G., Meynet G., Guseva N. G., Thuan T. X., 2006, A&A, 448, 955
 Izotov Y. I., Thuan T. X., Guseva N. G., 2007, ApJ, 671, 1297
 Izotov Y. I., Guseva N. G., Fricke K. J., Papaderos P., 2009, A&A, 503, 61
 Izotov Y. I., Guseva N. G., Thuan T. X., 2011, ApJ, 728, 161
 Izotov Y. I., Thuan T. X., Privon, G. 2012, MNRAS, 427, 1229
 Izotov Y. I., Stasińska G., Guseva N. G., 2013, A&A, 558, A57
 Izotov Y. I., Guseva N. G., Fricke K. J., Henkel C., 2014a, A&A, 561, A33
 Izotov Y. I., Thuan T. X., Guseva N. G., 2014b, MNRAS, 445, 778
 Izotov Y. I., Guseva N. G., Fricke K. J., Henkel C., 2015, MNRAS, 451, 2251
 Izotov Y. I., Orlitová I., Schaerer D., Thuan T. X., Verhamme A., Guseva N. G., Worseck G., 2016a, Nature, 529, 178
 Izotov Y. I., Schaerer D., Thuan T. X., Worseck G., Guseva N. G., Orlitová I., Verhamme A., 2016b, MNRAS, 461, 3683
 Izotov Y. I., Guseva N. G., Fricke K. J., Henkel C., 2016c, MNRAS, 462, 4427
 Izotov Y. I., Guseva N. G., Fricke K. J., Henkel C., Schaerer D., 2017, MNRAS, 467, 4118
 Jaskot A. E., Oey M. S., 2013, ApJ, 766, 91
 Kauffmann G. et al., 2003, MNRAS, 341, 33
 Leitet E., Bergvall N., Hayes M., Linné S., Zackrisson E., 2013, A&A, 553, A106
 Leitherer C. et al., 1999, ApJS, 123, 3
 Leitherer C., Ekström S., Meynet G., Schaerer D., Agienko

- K. B., Levesque E. M., 2014, *ApJS*, 212, 14
- Leitherer C., Hernandez S., Lee J. C., Oey M. S., 2016, *ApJ*, 823, 64
- Lejeune T., Buser R., Cuisinier F., 1997, *A&AS*, 125, 229
- Lodders K., 2010, in Coswami A., Reddy B. E., eds, *Principles and Perspectives in Cosmochemistry, Astrophysics and Space Science Proceedings*, Springer-Verlag Berlin Heidelberg, p. 379
- Loose H.-H., Thuan T. X., 1986, in Kunth D., Thuan T.X., Tran Thanh Van J., eds, *Star-forming dwarf galaxies and related objects*. Editions Frontières, Gif-sur-Yvette, p. 73
- Mitra S., Ferrara A., Choudhury T. R., 2013, *MNRAS*, 428, L1
- Nakajima K., Ouchi M., 2014, *MNRAS*, 442, 900
- Nakajima K., Ellis R. S., Iwata I., Inoue A. K., Kusakabe H., Ouchi M., Robertson B. E., 2016, *ApJ*, 831, L9
- Ouchi M. et al., 2009, *ApJ*, 706, 1136
- Planck Collaboration XVI, 2014, *A&A*, 571, A16
- Porter R. L., Ferland G. J., Storey P. J., Detisch M. J., 2012, *MNRAS*, 425, L28
- Porter R. L., Ferland G. J., Storey P. J., Detisch M. J., 2013, *MNRAS*, 433, L89
- Robertson B. E. et al., 2013, *ApJ*, 768, 71
- Robertson B. E., Ellis R. S., Furlanetto S. R., Dunlop J. S., 2015, *ApJL*, 802, L19
- Salpeter E. E., 1955, *ApJ*, 121, 161
- Stasińska G., Izotov Y., Morisset C., Guseva N., 2015, *A&A*, 576, A83
- Storey P. J., Hummer D. G., 1995, *MNRAS*, 272, 41
- Thuan T. X., 2008, in *Low-metallicity Star Formation: From the first Stars to Dwarf Galaxies*, eds. Hunt L. Madden S.C, Schneider R., Cambridge Univ. Press, Cambridge, p. 348
- Thuan T. X., Izotov Y. I., 1997, *ApJ*, 489, 623
- Verhamme A., Orlitová I., Schaerer D., Izotov Y., Worseck G., Thuan T. X., Guseva N., 2017, *A&A*, 597, 13
- Wise J. H., Cen R., 2009, *ApJ*, 693, 984
- Wright E. L., 2006, *PASP*, 118, 1711
- Yajima H., Choi J.-H., Nagamine K., 2011, *MNRAS*, 412, 411
- Yang H. et al., 2017, preprint arXiv:1701.01857